



## N<sub>2</sub>O production by high energy auroral electron precipitation

K. Semeniuk,<sup>1</sup> J. C. McConnell,<sup>1</sup> J. J. Jin,<sup>1</sup> J. R. Jarosz,<sup>1</sup> C. D. Boone,<sup>2</sup> and P. F. Bernath<sup>2,3</sup>

Received 7 December 2007; revised 25 May 2008; accepted 6 June 2008; published 19 August 2008.

[1] The Fourier transform spectrometer on SCISAT-1 observed enhanced concentrations of N<sub>2</sub>O above 50 km in February of 2004 and 2006 in the wintertime polar region. These anomalously high concentrations are associated with the transport of high levels of NO<sub>x</sub> in the polar night region from the upper mesosphere and lower thermosphere in both cases following sudden warming events in the middle of January. The NO<sub>x</sub> is produced by auroral electron precipitation. Simulations using a middle atmosphere chemistry climate model show significant amounts of N<sub>2</sub>O are produced in the upper mesosphere from the reaction of NO<sub>2</sub> and ground state atomic nitrogen. Thus, N<sub>2</sub>O acts as a signature of energetic electron precipitation. The model results exhibit polar-night-confined descent of NO<sub>x</sub> in the wake of sudden warmings and other dynamical regimes when the polar vortex intensifies at high latitudes in the mesosphere.

**Citation:** Semeniuk, K., J. C. McConnell, J. J. Jin, J. R. Jarosz, C. D. Boone, and P. F. Bernath (2008), N<sub>2</sub>O production by high energy auroral electron precipitation, *J. Geophys. Res.*, 113, D16302, doi:10.1029/2007JD009690.

### 1. Introduction

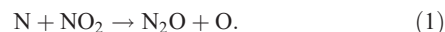
[2] It has been known for a long time that auroral precipitation generates copious amounts of NO<sub>x</sub> in the polar lower thermosphere and uppermost mesosphere [Callis, 1997]. In the winter time, during the long polar night and under suitable dynamical conditions significant amounts of NO<sub>x</sub> may be transported down to the lower mesosphere and upper stratosphere [e.g., Solomon *et al.*, 1982; Randall *et al.*, 2005; Hauchecorne *et al.*, 2007]. If the latter occurs then the auroral NO<sub>x</sub> can impact the ozone budget in the stratosphere [e.g., Rozanov *et al.*, 2005]. However, there is uncertainty about the source region of the NO<sub>x</sub>. For example, the descending NO<sub>x</sub> plume in early 2004 has been attributed to low energy electron precipitation in the lower thermosphere [Clilverd *et al.*, 2006]. Here we present chemical evidence that high energy electron precipitation ( $E > 100$  keV), which can produce NO<sub>x</sub> below 80 km, played a role during the 2004 event and during a similar event in 2006.

[3] Observations using the Fourier transform spectrometer (FTS) on SCISAT-1 for the Atmospheric Chemistry Experiment (ACE) also show N<sub>2</sub>O with volume mixing ratios between 4 and 5 ppbv descending below 60 km together with very high values of NO<sub>x</sub> in February 2004. Typical N<sub>2</sub>O mixing ratios are less than 0.5 ppbv above 50 km in the wintertime polar region due to descent of N<sub>2</sub>O depleted air from above. The NO<sub>x</sub> anomaly started its

descent in the upper mesosphere around mid January [Hauchecorne *et al.*, 2007] and appears to be associated with the occurrence of an exceptional major sudden stratospheric warming starting in late December 2003 [Manney *et al.*, 2005]. In 2006, the ACE-FTS observed another NO<sub>x</sub> anomaly descending below 60 km with N<sub>2</sub>O values of 2 to 3 ppbv in the same air mass. This descent was also associated with a sudden warming event in January 2006 [Manney *et al.*, 2008]. NO<sub>x</sub> concentrations were higher in 2004 compared to 2006 possibly due to the larger fluxes of high energy electrons stored in the magnetosphere [Baker *et al.*, 2004] in the wake of the October–November 2003 coronal mass ejection events. There is evidence of electron flux enhancement in observations from MEPED on NOAA-15, 16 and 17 during this time ([www.ngdc.noaa.gov/stp/NOAA/noaa\\_poes.html](http://www.ngdc.noaa.gov/stp/NOAA/noaa_poes.html)).

[4] In our study of NO<sub>x</sub> generation using ACE-FTS data we found that N<sub>2</sub>O-CH<sub>4</sub> correlations in the mesosphere yielded unusually large values implying excess amounts of N<sub>2</sub>O. Figure 1 (middle) shows the N<sub>2</sub>O-CH<sub>4</sub> correlation between 5.5 and 59.5 km and 55° and 80°N in the absence of excess NO<sub>x</sub> transport from the upper mesosphere. It exhibits the expected behavior as both methane and nitrous oxide have tropospheric sources and are destroyed in the stratosphere. In contrast, during periods of anomalous NO<sub>x</sub> descent in 2004 (Figure 1, left) and 2006 (Figure 1, right) there is a branch indicating excess N<sub>2</sub>O with respect to CH<sub>4</sub> at high altitudes. This indicates that there is an N<sub>2</sub>O source in the upper atmosphere, which appears not to have been identified before.

[5] N<sub>2</sub>O can be produced via the following reaction



<sup>1</sup>Department of Earth and Space Science and Engineering, York University, Toronto, Ontario, Canada.

<sup>2</sup>Department of Chemistry, University of Waterloo, Waterloo, Ontario, Canada.

<sup>3</sup>Department of Chemistry, University of York, Heslington, York, UK.

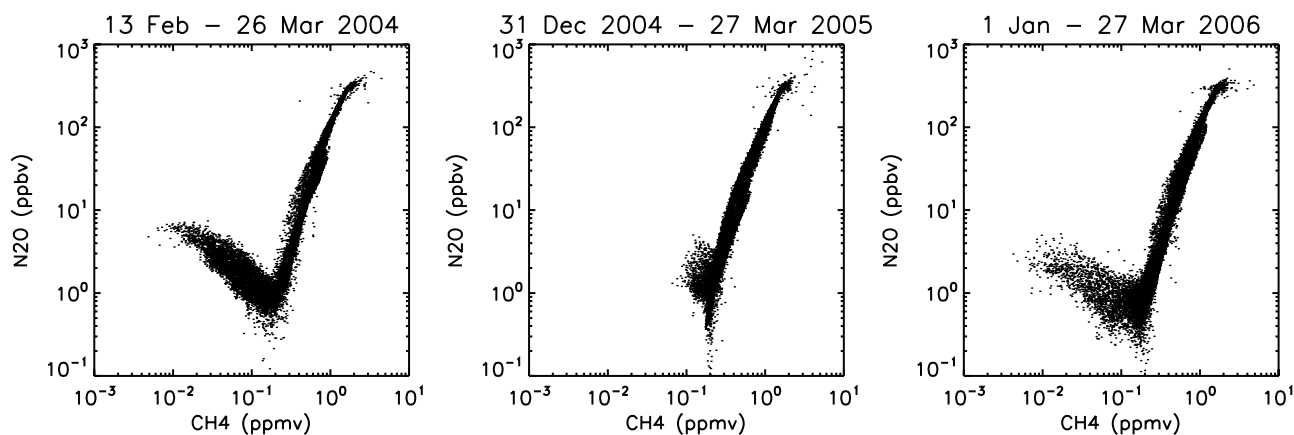


**Figure 1.** ACE-FTS CH<sub>4</sub> and N<sub>2</sub>O correlations between 5.5 and 59.5 km and 55° to 80°N.

Ionization processes such as solar proton events (SPEs) and aurorae, which produce both atomic nitrogen and NO can thus lead to the formation of N<sub>2</sub>O in the polar night, where NO is converted to NO<sub>2</sub>. Reaction (1) has not been previously included in our chemistry general circulation model (GCM). Given the lack of publications on this subject, it appears that this ionization-associated N<sub>2</sub>O source has not received much attention. To our knowledge ACE is the first to observe N<sub>2</sub>O originating in the upper mesosphere. The MIPAS instrument observed N<sub>2</sub>O production during the October–November 2003 SPEs [Funke *et al.*, 2008]. Simulations of N<sub>2</sub>O production during these SPEs using our model with reaction (1), presented by Funke *et al.* [2008], are in reasonable agreement with the observations.

[6] The high concentrations of atomic oxygen above 80 km keep the NO<sub>2</sub> amounts very small. Atomic nitrogen therefore has to occur below this altitude in order for N<sub>2</sub>O to be created. Transport of atomic nitrogen from above is excluded by its very short chemical lifetime (on the order of minutes at 80 km). Similarly horizontal transport of atomic nitrogen produced by photodissociation into the polar night is not a viable source. Thus, nitrous oxide acts as a marker for energetic electron precipitation (EEP) that penetrates into the upper mesosphere.

[7] Clilverd *et al.* [2006] concluded that the NO<sub>x</sub> anomaly in the mesosphere observed in early 2004 originated above 90 km. If this was the only source, then it would not be possible to observe any N<sub>2</sub>O as part of the same air mass. Nighttime photoionization of NO by scattered Lyman- $\alpha$  radiation produces NO<sup>+</sup> above 80 km but the ionization rate falls off rapidly at lower altitudes. Production of N(<sup>4</sup>S) can occur above 80 km via dissociative electron recombination but three body reactions of NO<sup>+</sup> leading to H<sub>2</sub>O cluster ions and eventually HO<sub>x</sub> dominate below 80 km [Brasseur and Solomon, 1986].

[8] The significance of major sudden stratospheric warmings for NO<sub>x</sub> transport in the northern hemisphere mesosphere stems from the opposing character of the circulation response in the two regions. Observations indicate that the mesosphere cools as the sudden warming develops in the stratosphere [e.g., Labitzke, 1972; Hoffmann *et al.*, 2002].

This behavior is also captured by GCMs [e.g., Miyoshi, 2003]. The cooling is associated with an intensification of the polar vortex in the upper mesosphere for reasons discussed below. A strong polar vortex confines the air mass in its interior, which encloses the polar night region, and reduces photolytic NO<sub>x</sub> loss.

[9] We investigate auroral NO<sub>x</sub> and N<sub>2</sub>O production using the Canadian Middle Atmospheric Model (CMAM) as in the work of Semeniuk *et al.* [2005] but with reaction (1) and its branches included. The version of CMAM that we use here has a T31 spectral resolution with 71 sigma-pressure hybrid levels extending from the surface to about 95 km. There is a nonzonal sponge layer in the upper two pressure scale heights of the model (i.e., above 80 km). A more detailed description of the model is given by Jonsson *et al.* [2004] and Fomichev *et al.* [2007] and references therein.

[10] For the simulations presented here we have modified the neutral photochemistry scheme to include the ionization production of NO<sub>x</sub>, HO<sub>x</sub> and O<sub>x</sub> and a new solver. Our model does not include ion chemistry. The solver has a very high degree of optimization such that it takes  $O(n)$  operations to invert the Jacobian matrix instead of  $O(n^3)$  where  $n$  is the number of species. For the formulation based on Gaussian elimination, this is achieved by species re-ordering such that the nonzero elements populate the lower rows of the sparse Jacobian in order to minimize the fill-in during the elimination and therefore preserve the sparse structure. The solver code is automatically generated so that changes in the specified reactions and species are straightforward to implement. This preprocessing approach is similar to that of Damian *et al.* [2002] but has a different algorithm since their formulation is based on LU decomposition of the Jacobian. The solver generator was developed by one of the authors (J. R. Jarosz) and a paper describing it is in preparation.

[11] We conducted six two-month simulations from initial conditions taken from the beginning of January of several consecutive model years corresponding to the 2005–2008 period from a WMO Ref2 simulation [Eyring *et al.*, 2006]. This choice was based on the realism of the model distribution of chemical constituents and circulation regime.

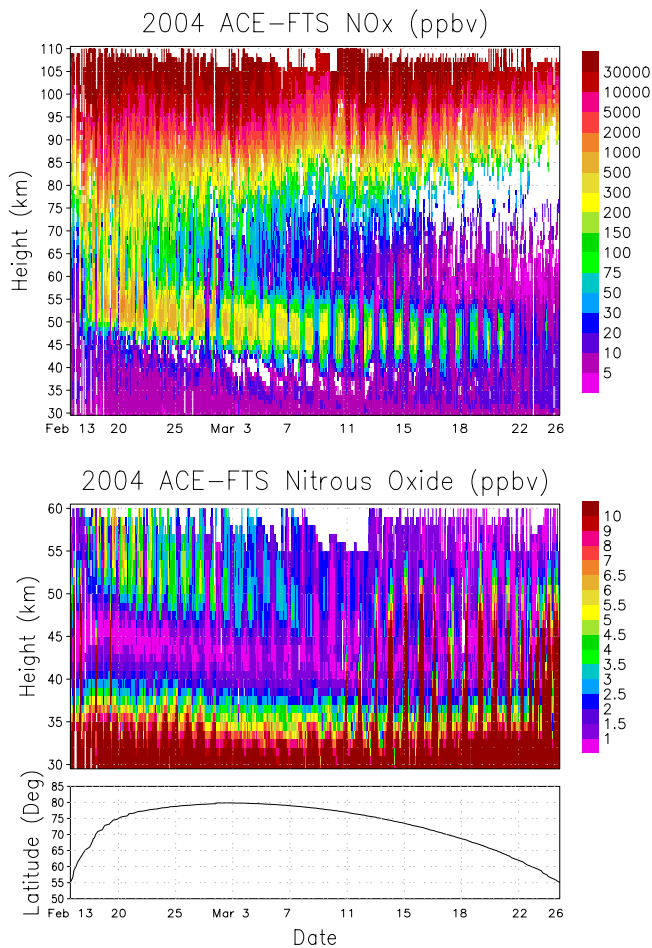


**Figure 2.** Time series of ACE-FTS NO<sub>x</sub> and N<sub>2</sub>O in early 2004 for sequential orbits.

CMAM develops major sudden stratospheric warmings (SSWs) in the northern hemisphere roughly every other year. So the choice of initial states had a high probability of developing an SSW event. The initial states were used for runs with two choices of the reaction rate for reaction (1). This essentially doubled the number of members in our ensemble since the dynamics respond to small changes in chemical composition.

[12] These simulations were free running and not data assimilation cycles so they are not expected to capture the weather of early 2004 and 2006. However, major sudden warmings have typical characteristics that are captured by GCMs [Charlton *et al.*, 2007]. So analyzing transport by model SSWs is worthwhile. One of our simulations, Case I, developed a persistent major sudden warming and had exceptional polar-night-confined descent that we believe is similar to that which occurred in the atmosphere in January and February of 2004 [Manney *et al.*, 2005]. The timing and details, however, differ from the observations. Another simulation, Case II, developed a polar-night-confined transport feature but in the absence of a major warming. Case II was not an expected outcome of our simulations. It occurred only for one of the choices of reaction rate, which indicates

that it is a rare type of event and our ensemble is too small to characterize its frequency.

## 2. Observations

[13] SCISAT-1 is a small Canadian satellite that was launched on 12 August 2003 into a 74 degree inclined orbit at 650 km altitude [Bernath *et al.*, 2005]. The satellite carries three instruments operating in occultation mode with a shared field of view to take advantage of the high precision of the solar occultation technique. The ACE instrument is an infrared Fourier transform spectrometer (FTS) with a spectral resolution of 0.02 cm<sup>-1</sup> from 750 to 4400 cm<sup>-1</sup>. The instrument is self-calibrating as low Sun measurements (i.e., made through the atmosphere) of solar spectra are divided by exo-atmospheric solar spectra from the same occultation. The orbit yields tropical to high latitude occultations in both hemispheres with a vertical resolution of 3–4 km.

[14] Figures 2 and 3 show altitude versus time plots of NO<sub>x</sub> (defined as NO + NO<sub>2</sub>) and N<sub>2</sub>O observed by ACE in 2004 and 2006. The plots are sequential composites of all profiles and reflect the variation around a latitude circle and the gradual evolution of the orbit (shown in the bottom panel). Concentrations of NO<sub>x</sub> exceeding 30 ppmv are evident at 100 km. In mid-February of 2004 values of

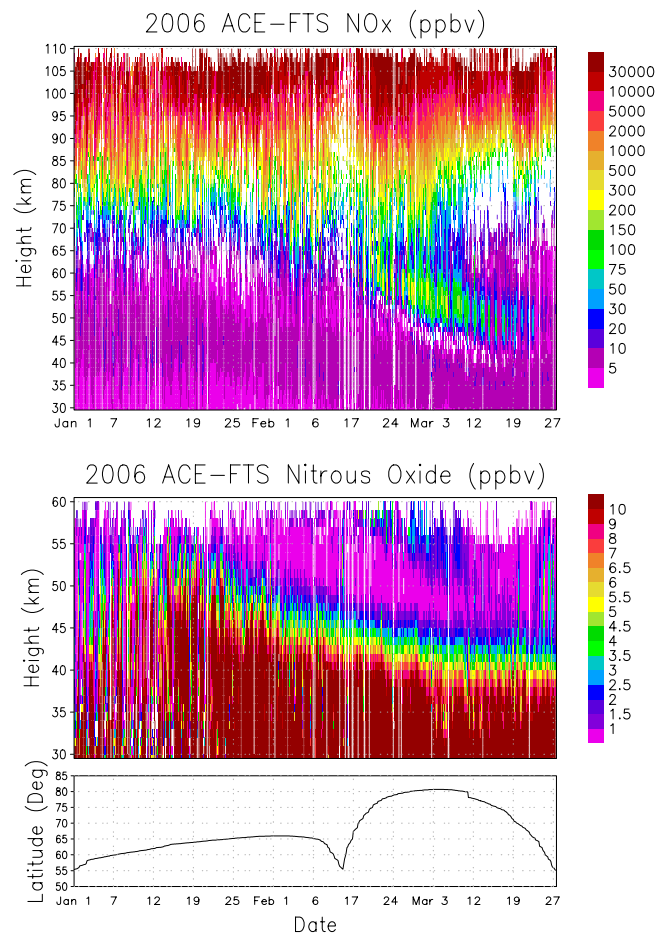


**Figure 3.** Time series of ACE-FTS NO<sub>x</sub> and N<sub>2</sub>O in early 2006 for sequential orbits.

5 ppmv were present at 85 km, indicating production below 100 km since the separation in altitude is about three density scale heights. The N<sub>2</sub>O retrieval generally extends only up to 60 km since the signal to noise ratio above is typically too small. However, it is evident that the N<sub>2</sub>O is descending from above together with the same air mass as the NO<sub>x</sub>.

### 3. Description of the Model Experiment

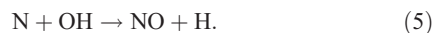
[15] We use electron flux observations by the MEPED detectors on board NOAA-15, 16 and 17 to infer an electron energy deposition. Since the model lid does not extend above 100 km, only the 30–100 keV, 100–300 keV and 300–2500 keV channel fluxes are considered. Even though high amounts of NO<sub>x</sub> are formed above 100 km by low energy electron precipitation, it is likely that NO<sub>x</sub> produced below 100 km accounts for most of the observed anomaly. The potential for NO<sub>x</sub> loss by exposure to sunlight increases with altitude. This is due in part to the increasing amplitude of waves at higher altitudes on account of decreasing density, which produce significant meridional excursions of air parcels into sunlight. It is also due to the increase of photolysis rates with height for solar zenith angles over 90°. Hence, the longer the duration of the descent the less likely that NO<sub>x</sub>-rich air parcels are able to remain confined to the polar night and NO<sub>x</sub> loss occurs via photolysis of NO followed by the reaction of the resulting N with NO viz.,



It is possible for the N produced by photolysis to be recycled into NO via



and



Reaction (4) is very slow at low mesospheric temperatures and reaction (5) is limited by the availability of OH especially above 80 km due to large atomic oxygen concentrations. In spite of these reactions, there is a net loss from daylight exposure of NO.

[16] A vertical energy deposition profile was derived by compositing, daily, the electron flux data and taking peak flux values from twelve 30° longitudinal sectors. The average of these twelve peak flux values was used for subsequent calculations. The dependence of the flux on energy was approximated by a piece-wise exponential fit following *Callis et al.* [1998]. The energy deposition was obtained using the range-energy expression from *Gledhill* [1973].

[17] To obtain a 3D distribution of the electron energy deposition the vertical energy deposition profile was multiplied by a parametrized auroral oval. The auroral oval is a modified version of the scheme from *Holzworth and Meng* [1975] based on the formulation of *Feldstein* [1963]. The

modification for the horizontal distribution,  $H$ , was as follows:

$$H(\phi, \theta) = \begin{cases} \exp\left(-((\theta_g(\phi, \theta) - \theta_c)/\delta\theta_p)^2\right), & \text{if } \theta_g > \theta_c \\ \exp\left(-((\theta_g(\phi, \theta) - \theta_c)/\delta\theta_e)^2\right), & \text{if } \theta_g \leq \theta_c \end{cases} \quad (6)$$

$$\begin{aligned} \theta_c &= \theta_e + 0.3(\theta_p - \theta_e) \\ \delta\theta_p &= 2(\theta_p - \theta_c) \\ \delta\theta_e &= (\theta_c - \theta_e) \end{aligned} \quad (7)$$

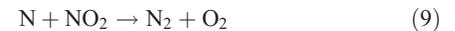
where  $\theta_e$  and  $\theta_p$  are the equatorial and polar corrected geomagnetic latitude limits of the auroral oval, respectively, from the *Holzworth and Meng* [1975] scheme. The map from geographic longitude ( $\phi$ ) and latitude ( $\theta$ ) on the model grid to corrected geomagnetic latitude ( $\theta_g(\phi, \theta)$ ) was calculated offline. This modification was made to improve the realism of the auroral oval distribution.

[18] Hourly values of the AE index (from [swdcwww.kugi.kyoto-u.ac.jp](http://swdcwww.kugi.kyoto-u.ac.jp)) were used to specify the size of the oval using the relation for the Q index from *Starkov* [1981]. The orientation of the oval follows the Sun.

[19] This formulation has a number of biases. It overestimates the electron flux, but not excessively as seen in the NO<sub>x</sub> values obtained a posteriori. It also produces an auroral oval that is too small and confined to the polar region for large geomagnetic storm events. The parameterized auroral oval resets Q values to six when they exceed this number, so that more NO<sub>x</sub> is deposited in the polar night than should be.

[20] The ionization rate and the production of NO<sub>x</sub>, HO<sub>x</sub> and O<sub>x</sub> was parametrized using the energy deposition as in the work of *Semeniuk et al.* [2005]. Figure 4 (top) shows the hourly NO<sub>x</sub> total column production in the geomagnetic polar cap. The average daily column production is  $7.9 \times 10^{13}$  molecules per cm<sup>2</sup>. There is significant ionization below 80 km for most of the simulation period (Figure 4, bottom).

[21] The CMAM chemistry package was modified to include reaction (1) and its branches. The reaction rate is from *Wennberg et al.* [1994] and is four times faster than that of *Clyne and Ono* [1982]. Other possible branches for reaction (1) are



*Wennberg et al.* [1994] note that a 2:1 branching ratio for reaction (1) and each of reactions (8) and (9) is not excluded by their experiments. For Case I only the N<sub>2</sub>O branch was included, with the full reaction rate. For Case II we assumed that the branch that produces N<sub>2</sub>O is 50% of the total and reactions (8) and (9) each account for 25%.

## 4. Results

### 4.1. Meteorology

[22] Six January through February simulations were conducted. Two runs (Case I and II) exhibited an anomalous

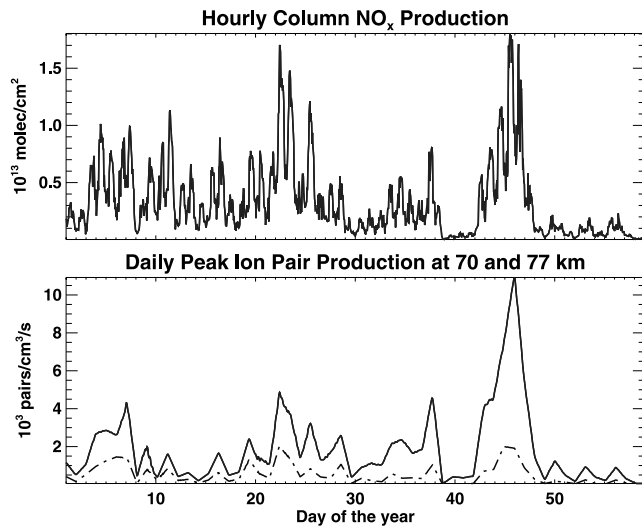


**Figure 4.** (top) Northern hemisphere hourly total column NO<sub>x</sub> production poleward of 63° geomagnetic latitude in 2004. (bottom) Maximum daily ion pair production rate on the 70 km (dash-dot) and 77 km (solid) surface for the same period.

descent pattern with large values of NO<sub>x</sub> reaching the polar stratopause region. One of these events (Case I) occurred towards the end of a sustained major stratospheric warming. As noted in the introduction, observations for 2004 and 2006 indicate that polar-night-confined descent of NO<sub>x</sub> occurs in association with major sudden warmings [Randall et al., 2006].

[23] Figure 5 shows the evolution of the Case I CMAM zonal mean zonal wind and temperature deviation from the MSIS90 climatology [Hedin, 1991] at 80°N. A major warming develops in early January and the stratospheric

winds do not fully recover even by the end of February. A high latitude intensification of the polar vortex occurs in the mesosphere due to the weakened/reversed vortex winds in the stratosphere. This results from the increased filtering of gravity waves with easterly phase speeds and reduced filtering of those with westerly phase speeds by the anomalous stratospheric winds. In this case the typically strong easterly gravity wave drag in the mesosphere, which suppresses high latitude westerly zonal winds, becomes much weaker or even westerly depending on the magnitude of the stratospheric easterlies [e.g., Holton, 1982].

[24] The cooling above 60 km between the 10th and 20th of January is part of the early stage of the major warming. The warming is initially concentrated in the upper stratosphere and then descends to lower altitudes. The descent of the region of warming and the easterly zonal wind is due to the formation of a zero wind line which leads to planetary Rossby wave breaking below it. This, in turn, produces easterlies and moves the zero wind line downward [e.g., Zhou et al., 2001].

[25] A mesospheric cooling develops above the region of stratospheric warming since the polar vortex is reversed, first in the upper stratosphere and subsequently at lower altitudes. Since the stratospheric easterlies are coupled with a reversal in the sign of the gravity wave drag in the mesosphere, the meridional diabatic circulation is reduced or even reversed in the polar region. This leads to less dynamical heating and lower temperatures. As the region of easterlies descends, the cooling region above them follows since the diabatic downwelling and the associated heating are reduced at lower altitudes.

[26] There is also a warming in the upper mesosphere in February. The temperature anomaly pattern is similar to that inferred from SABER temperatures by Hauchecorne et al. [2007] (see their Figure 3). This feature is associated with enhanced diabatic downwelling that develops towards the end of the major sudden warming event as the stratospheric

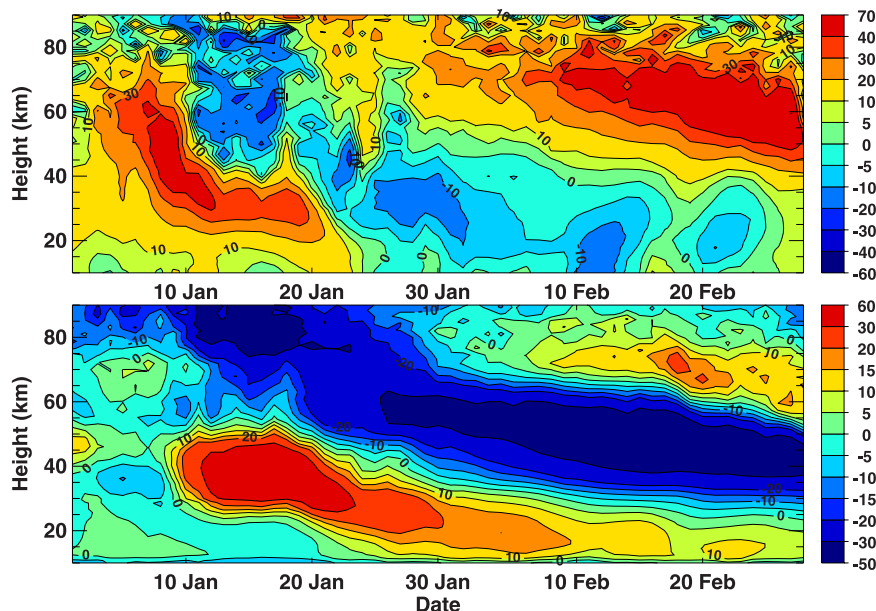


**Figure 5.** Case I: CMAM zonal wind (m/s) (top) and temperature deviation (K) from MSIS90 (bottom) at 80°N.

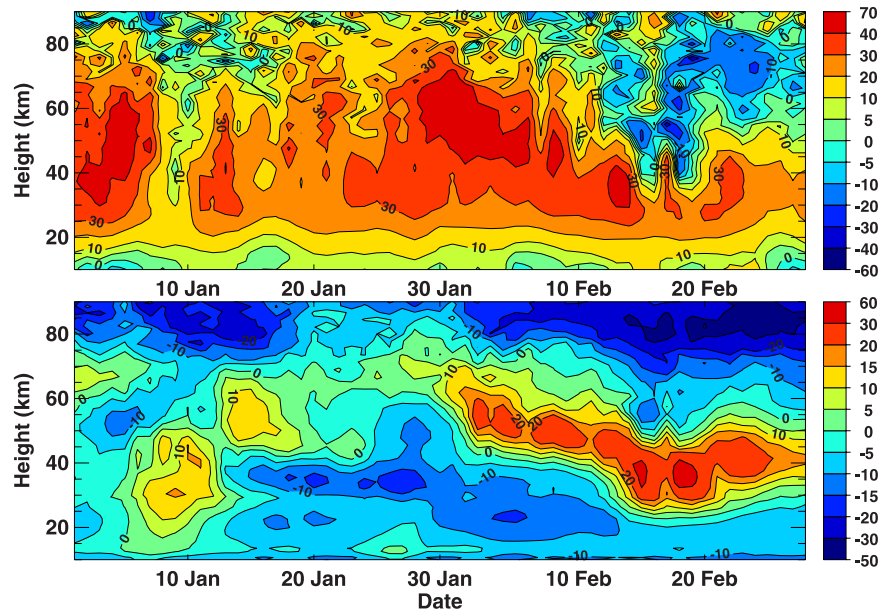


**Figure 6.** Case II: CMAM zonal wind (m/s) (top) and temperature deviation (K) from MSIS90 (bottom) at 80°N.

westerlies recover and easterly gravity wave drag increases in the mesosphere. This change in the dynamical regime is reflected in the transport of chemical tracers. The presence of a strong polar vortex in the high latitude mesosphere during this time, which results from the earlier stages of the warming event, produces a high degree of polar night confinement of the descending air mass and allows high NO<sub>x</sub> values to reach the stratosphere without photolysis of NO. In addition, the enhanced temperatures due to dynamical heating should allow for increased recycling of N produced by exposure to sunlight back into NO via reaction (4), which is much more efficient at higher temperatures.

[27] The evolution for Case II is shown in Figure 6. In this case, there is no evidence of a major warming during

the period of the run, but a minor warming develops around January the 10th. This minor warming event appears to not last past the middle of the month. However, the vortex in the mesosphere is disturbed until late January when it intensifies between 50 km and 70 km. As with Case I, the enhanced vortex in the mesosphere is accompanied by increased descent and associated diabatic heating, which appears as the band of higher temperatures around 50 km starting in February. The origins of this mesosphere vortex anomaly are not readily apparent but there is a significant intensification of zonal wave number two in late January in the upper stratosphere and lower mesosphere (not shown). This is suggestive of a preconditioning event that leads to the warming in February. Further analysis of the this vortex

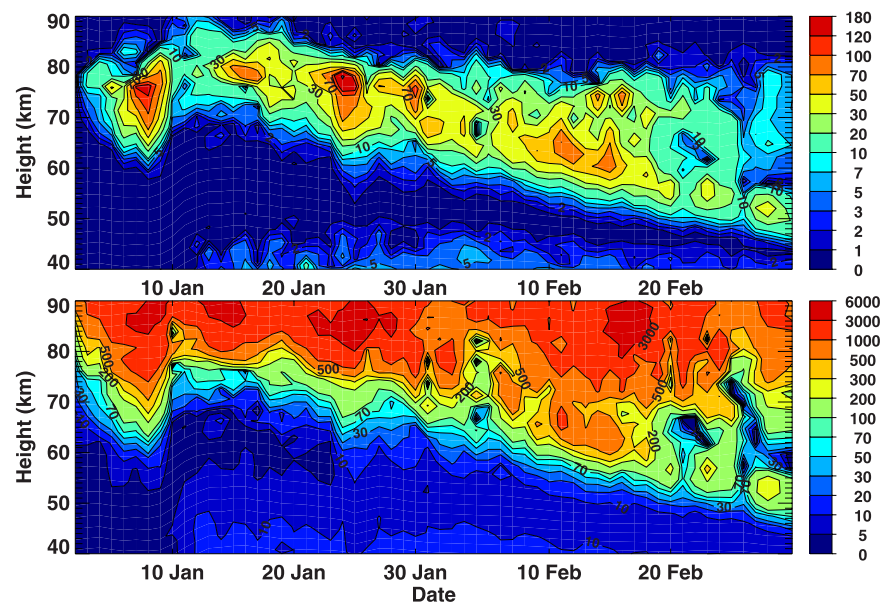


**Figure 7.** Case I: N<sub>2</sub>O (ppbv) (top) and NO<sub>x</sub> (ppbv) (bottom) at 80°N and 0°E versus time.

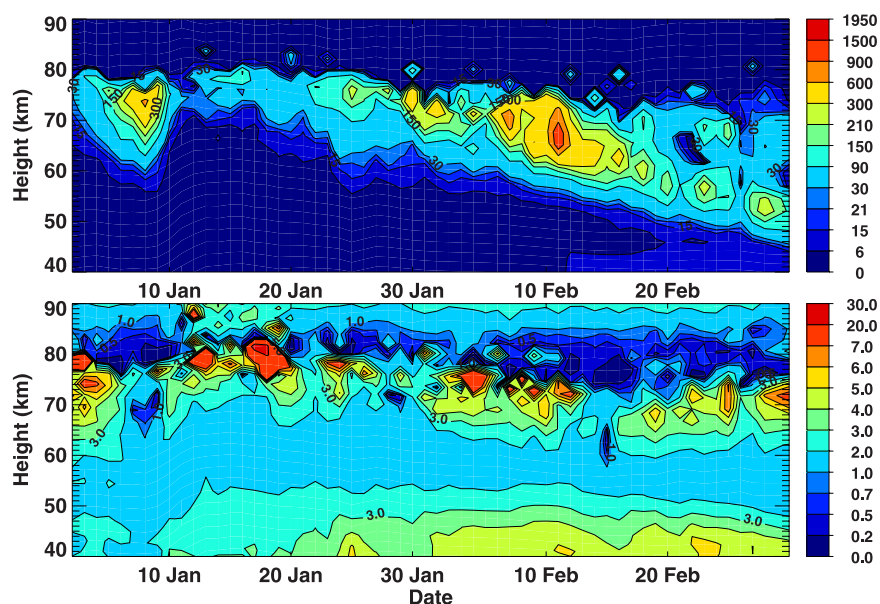


**Figure 8.** Case I: NO<sub>2</sub> (ppbv) (top) and O<sub>3</sub> (ppmv) (bottom) at 80°N and 0°E versus time.

disturbance is beyond the scope of the work presented here and will be explored in a later paper. Since CMAM does a reasonable job simulating synoptic and planetary scale dynamics, there is good reason to expect such vortex regimes to develop in the real atmosphere.

#### 4.2. Chemical Fields

[28] Figure 7 shows altitude versus time plots of NO<sub>x</sub> and N<sub>2</sub>O for 80°N, chosen to be representative of the polar fields. The values of NO<sub>x</sub> that descend below 60 km are over 0.2 ppmv which is in the range seen by the ACE-FTS in 2004. Above 80 km peak values of NO<sub>x</sub> over 3 ppmv are present. These are not excessively high given the auroral electron ionization prescribed. The ACE-FTS recorded NO values as high as 10 ppmv at 90 km in early 2004. In addition, these NO<sub>x</sub> concentrations are partly a reflection of enhanced polar night confinement above 80 km in the model. The nonzonal sponge layer significantly reduces the variance of the meridional velocity associated with Rossby waves and tides and hence the air parcel excursions from polar night into sunlit regions.

[29] In contrast, N<sub>2</sub>O has peak concentrations below 60 km over 30 ppbv, which is about one order of magnitude larger than the observations. A part of this disagreement could possibly be due to the absence of other branches of reaction (1) in this model run, which would reduce the amount of N<sub>2</sub>O produced by a factor of two. But another significant factor is that NO<sub>2</sub> (Figure 8, top) forms in large quantities in the model about 8 km higher than in observations by GOMOS (see the altitude versus time distribution of NO<sub>2</sub> at 80°N shown in Figure 1 of *Hauchecorne et al.* [2007]). This is due to the large amounts of O<sub>3</sub> produced in the region above 70 km (Figure 8, bottom) and the warmer temperatures. As a result there is more exposure of NO<sub>2</sub> to ionization-produced ground state atomic nitrogen, which varies rapidly with altitude, and the formation of N<sub>2</sub>O by reaction (1) is increased.

[30] Values of O<sub>3</sub> as high as 40 ppmv occur sporadically in the model high latitudes around 80 km in simulations without electron ionization (not shown). These ozone spikes probably reflect rapid transport from above where O<sub>x</sub> mixing ratios are very large. The model ozone concentrations are reduced by HO<sub>x</sub> generated by ionization, but by less than 25%. The ozone budget may also be impacted by geocoronal Lyman- $\alpha$  production of NO<sup>+</sup> in the polar night. The NO<sup>+</sup> generates HO<sub>x</sub> via three body reactions in the region where ozone production maximizes around 80 km. However, this relatively minor HO<sub>x</sub> source is not included in the model.

[31] Transport differences between the model and the real atmosphere also appear to be responsible for the high ozone values in this region. The observations by GOMOS in 2004 [*Hauchecorne et al.*, 2007] show very little NO<sub>2</sub> and O<sub>3</sub> in the polar night above 70 km before and after the mid-January descent event. This suggests that air parcels above 70 km experienced more exposure to sunlight compared to the model simulations.

[32] Below 85 km O<sub>3</sub> is produced efficiently via the three body reaction of atomic oxygen with molecular oxygen. This is especially true in the high latitude wintertime where diabatic descent transports atomic oxygen to the mesopause region from the lower thermosphere. It is through rapid reaction with remaining atomic oxygen, other species (e.g., H and OH) and photolysis that ozone is reduced to the range of a few ppmv. All else being equal, lower levels of sunlight exposure of polar air parcels result in higher ozone concentrations. These conditions also lead to increased NO<sub>2</sub> concentrations due to NO reacting with more abundant O<sub>3</sub> and reduced photolytic loss. The abundance of NO<sub>2</sub> in the model at higher altitudes yields significantly greater amounts of N<sub>2</sub>O.

[33] Figure 9 shows N<sub>2</sub>O and NO<sub>2</sub> for Case II. A descending anomaly structure develops in late January and reaches 50 km by February 10. The concentrations

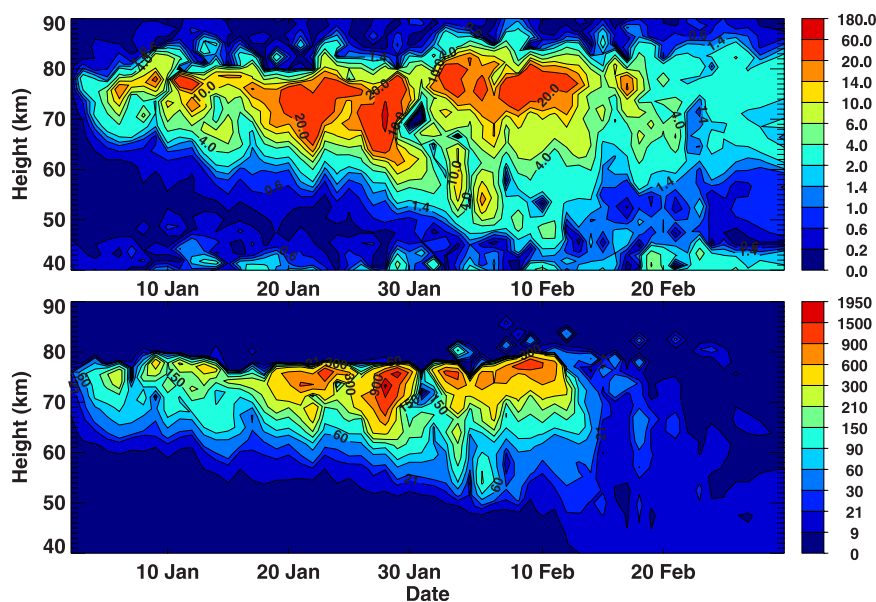


**Figure 9.** Case II: N<sub>2</sub>O (ppbv) (top) and NO<sub>2</sub> (ppbv) (bottom) at 80°N and 0°E versus time.

of N<sub>2</sub>O are roughly half of those in Case I due to the change in reaction rate required by the additional branches of reaction (1).

## 5. Discussion

[34] The parameterized ionization by auroral electron precipitation used here appears to produce NO<sub>x</sub> values in qualitative agreement with observations. Specific transport features seen in observations such as the high values of NO<sub>x</sub> around 55 km in 2004 are not captured by such free running climate model simulations. We have verified that the in situ N(<sup>4</sup>S) source from ionization is essential to the formation of N<sub>2</sub>O. A re-run of Case I with the ionization production of N(<sup>4</sup>S) turned off results in negligible N<sub>2</sub>O concentrations that do not exceed 0.3 ppbv anywhere in the middle and upper mesosphere (not shown). The N(<sup>4</sup>S) produced by photodissociation of NO has concentrations of less than 0.3 ppbv below 80 km at the edge of the polar night during daytime where it can be exposed to polar night NO<sub>2</sub> through mixing.

[35] For the levels of NO<sub>x</sub> produced in the model, the amount of N<sub>2</sub>O produced is larger than the ACE-FTS observations in 2004 and 2006. This difference depends on whether the other branches of reaction (1) are included in the model chemistry scheme, in which case the production is reduced by half. More importantly, the production depends on the transport behavior in the upper mesosphere and lower thermosphere. The GOMOS observations indicate some process that suppresses both O<sub>3</sub> and the associated NO<sub>2</sub> formation above 70 km. This could be horizontal excursion of air parcels into daylight, which extends to 70°N by the middle of January. It could also be due to much more rapid descent of air above 70 km during the final stages of the sudden warming event in the real atmosphere as compared to the model.

[36] A model limitation that plays a significant role in the excess N<sub>2</sub>O production is the treatment of photolysis rates.

The precalculated photolysis rates, which take sphericity into account, are cut off for solar zenith angles greater than 95°. As a result photolytic destruction of NO<sub>2</sub> above 60 km is underestimated. We repeated the Case I run using photolysis rates with the cut off solar zenith angle moved to 100° (not shown). A similar major warming event and associated transport pattern developed in this run as well. The N<sub>2</sub>O mixing ratios dropped by over 33%. However, the altitude of the onset of NO<sub>2</sub> formation in January was not reduced. This supports the case for mixing processes in the model above 70 km being different from the atmosphere. It is also possible that geocoronal Lyman- $\alpha$  radiation is contributing to HO<sub>x</sub> production from NO<sup>+</sup> in the polar night around 80 km. This is a sink for ozone that is missing in the model.

[37] From the CMAM simulations there is a clear link between the occurrence of major sudden warmings and polar-night-confined transport of NO<sub>x</sub> from the mesopause region to the upper stratosphere. This is related to the formation of high latitude westerlies in the mesosphere and the surge of polar downwelling that develops towards the end of the warming event as stratospheric westerlies recover. However, these transport events are not constrained to occur in the recovery stage of major sudden warmings as demonstrated by Case II. In Case II the polar vortex in the mesosphere also intensifies closer to the pole, resulting in a narrower latitudinal distribution compared to the climatological case, which facilitates polar-night-confined descent.

[38] The set of simulations conducted here using CMAM are not sufficient to determine what probability there is for the occurrence of regimes similar to Case II. In addition, given that GCMs have problems capturing sudden warming frequency [Charlton *et al.*, 2007], even a more comprehensive set of simulations may not yield the correct answer as pertains to the atmosphere. More detailed analyses of CMAM sudden warming characteristics are given by Chaffey and Fyfe [2001] and Manson *et al.* [2006].

[39] The behavior of CCMs in the mesosphere and above is dependent on the parametrized nonorographic gravity wave drag. Density decrease with height increases the amplitude and hence the impact of gravity waves on the circulation and temperature. Models are only able to resolve a fraction of the gravity wave spectrum [e.g., *Hamilton et al.*, 1999]. To determine if we could imitate the observed transport regime better, additional simulations were performed with parametrized nonorographic gravity wave drag settings that deposit more momentum at higher altitudes. Following the tests by *McLandress and Scinocca* [2005] the CMAM nonorographic gravity wave drag scheme was made to behave more like the Hines parametrization instead of the Warner-McIntyre parametrization. We were able to capture a case with a major sudden warming. However, there was no noticeable drop in the altitude of the onset of NO<sub>2</sub> formation and hence no significant change in the amount of N<sub>2</sub>O produced. Due to an increase in the short timescale meridional wind variance between 50 and 70 km the descending NO<sub>x</sub> anomaly was eroded by daylight exposure and mixing before it could reach the stratopause. It is possible that the polar air mass is still not sufficiently disturbed between 70 and 80 km for NO<sub>2</sub> formation to be suppressed by exposure to daylight in the model compared to the real atmosphere. This line of investigation leaves open questions and requires additional work.

[40] We also varied the fraction of N(<sup>4</sup>S) and N(<sup>2</sup>D) produced by the ionization scheme since NO<sub>x</sub> production depends on the yield of N(<sup>4</sup>S) [*Rusch et al.*, 1981]. But the results were not found to be particularly sensitive to this.

## 6. Conclusions

[41] Our model results confirm that N<sub>2</sub>O is produced in the upper mesosphere by EEP in the polar night and transported to the stratopause region during major SSW events. Thus, N<sub>2</sub>O acts as a signature of EEP below 80 km. In addition, we find that high values of NO<sub>x</sub> can be transported into the lower polar mesosphere without a major SSW. The dynamics of these events require additional study and they appear to be rare.

[42] Based on the GOMOS observations of NO<sub>2</sub> in January 2004 there must have been a nonnegligible amount of high energy electron precipitation that penetrated to 70 km and below. Ground state atomic nitrogen is too short lived to be transported from above and has to be generated in situ. The MEPED electron flux measurements show a significant amount of high energy electron precipitation for early 2004.

[43] The simulations presented here point to the possibility of much higher N<sub>2</sub>O formation if NO<sub>2</sub> is available between 70 and 80 km during high energy electron precipitation events. It is not clear, however, if such conditions can develop in the atmosphere and they do not in existing observations. The MEPED electron flux data, when analyzed over its whole timespan, indicates that high energy electron precipitation that can penetrate below 80 km is not rare. Hence, it is possible that nitrous oxide is being produced on a regular basis in the upper mesosphere and it is worthwhile for N<sub>2</sub>O retrievals to be performed above 60 km.

[44] **Acknowledgments.** The authors would like to thank the Natural Sciences and Engineering Research Council of Canada, the Canadian Foundation for Climate and Atmospheric Sciences, the Canadian Foundation for Innovation and the Ontario Innovation Trust. The ACE mission is funded primarily by the Canadian Space Agency. We are also grateful for the useful suggestions of Charles McLandress and the comments of the reviewers.

## References

- Baker, D. N., S. G. Kanekal, X. Li, S. P. Monk, J. Goldstein, and J. L. Burch (2004), An extreme distortion of the Van Allen belt arising from the 'Halloween' solar storm in 2003, *Nature*, *432*, 878–881.
- Bernath, P. F., et al. (2005), Atmospheric Chemistry Experiment (ACE): Mission overview, *Geophys. Res. Lett.*, *32*, L15S01, doi:10.1029/2005GL022386.
- Brasseur, G. P., and S. Solomon (1986), *Aeronomy of the Middle Atmosphere*, 452 pp., D. Reidel, Norwell, Mass.
- Callis, L. B. (1997), Odd nitrogen formed by energetic particle precipitation as calculated from Tiros data, *Geophys. Res. Lett.*, *24*, 3237–3240.
- Callis, L. B., M. Natarajan, J. D. Lambeth, and D. N. Baker (1998), Solar atmospheric coupling by electrons (SOLACE) 2. Calculated stratospheric effects of precipitating electrons, 1978–1988, *J. Geophys. Res.*, *103*, 28,421–28,438.
- Chaffey, J. D., and J. C. Fyfe (2001), Arctic polar vortex variability in the Canadian Middle Atmosphere Model, *Atmos. Ocean*, *39*, 457–469.
- Charlton, A. J., L. M. Polvani, J. Perlwitz, F. Sassi, E. Manzini, K. Shibata, S. Pawson, J. E. Nielsen, and D. Rind (2007), A new look at stratospheric sudden warmings. Part II: Evaluation of numerical model simulations, *J. Clim.*, *20*, 470–488.
- Clilverd, M. A., A. Seppälä, C. J. Rodger, P. Verronen, and N. R. Thomson (2006), Ionospheric evidence of thermosphere-to-stratosphere descent of polar NO<sub>x</sub>, *Geophys. Res. Lett.*, *33*, L19811, doi:10.1029/2006GL026727.
- Clyne, M. A. A., and Y. Ono (1982), Determination of the rate constant of reaction of N(<sup>4</sup>S<sub>3/2</sub>) with NO<sub>2</sub> using resonance fluorescence in a discharge flow system, *Chem. Phys.*, *69*, 381–388.
- Damian, V., A. Sandu, M. Damian, F. Potra, and G. R. Carmichael (2002), The kinetic preprocessor KPP - A software environment for solving chemical kinetics, *Comp. Chem. Eng.*, *26*(11), 1567–1579.
- Eyring, V., et al. (2006), Multimodel projections of stratospheric ozone in the 21st century, *J. Geophys. Res.*, *112*, D16303, doi:10.1029/2006JD008332.
- Feldstein, Y. I. (1963), On morphology of auroral and magnetic disturbances at high latitudes, *Geomagn. Aeron. USSR*, *3*, 183–192.
- Fomichev, V. I., A. I. Jonsson, J. de Grandpré, S. R. Beagley, C. McLandress, K. Semeniuk, and T. G. Shepherd (2007), Response of the middle atmosphere to CO<sub>2</sub> doubling: Results from the Canadian Middle Atmosphere Model, *J. Clim.*, *20*, 1121–1144, doi:10.1175/JCLI4030.1.
- Funke, B., M. García-Comas, M. López-Puertas, N. Glatthor, G. P. Stiller, T. von Clarmann, K. Semeniuk, and J. C. McConnell (2008), Enhancement of N<sub>2</sub>O during the October–November 2003 solar proton events, *Atmos. Chem. Phys. Discuss.*, *8*, 4669–4691.
- Gledhill, J. A. (1973), The range-energy relation for 0.1–600 keV electrons, *J. Phys. A Math Nucl. Gen.*, *6*, 1420–1428.
- Hamilton, K., R. J. Wilson, and R. Hemler (1999), Middle atmosphere simulated with high vertical and horizontal resolution versions of a GCM: Improvement in the cold pole bias and generation of a QBO-like oscillation in the tropics, *J. Atmos. Sci.*, *56*, 3829–3846.
- Hauchecorne, A., J.-L. Bertaux, F. Dalaudier, J. M. Russell III, M. G. Mlynczak, E. Kyrölä, and D. Fussen (2007), Large increase of NO<sub>2</sub> in the polar mesosphere in January–February 2004: Evidence of a dynamical origin from GOMOS/ENVISAT and SABER/TIMED data, *Geophys. Res. Lett.*, *34*, L03810, doi:10.1029/2006GL027628.
- Hedin, A. E. (1991), Extension of the MSIS thermosphere model into the middle and lower atmosphere, *J. Geophys. Res.*, *96*, 1159.
- Hoffmann, P., W. Singer, and D. Keuer (2002), Variability of the mesospheric wind field at middle and Arctic latitudes in winter and its relation to stratospheric circulation disturbances, *J. Atmos. Sol. Terr. Phys.*, *64*, 1229–1240.
- Holton, J. R. (1982), The role of gravity wave induced drag and diffusion in the momentum budget of the mesosphere, *J. Atmos. Sci.*, *39*, 791–799.
- Holzworth, R. H., and C.-I. Meng (1975), Mathematical representation of the auroral oval, *Geophys. Res. Lett.*, *2*, 377.
- Jonsson, A. I., J. de Grandpré, V. I. Fomichev, J. C. McConnell, and S. R. Beagley (2004), Doubled CO<sub>2</sub>-induced cooling in the middle atmosphere: Photochemical analysis of the ozone radiative feedback, *J. Geophys. Res.*, *109*, D24103, doi:10.1029/2004JD005093.
- Labitzke, K. (1972), Temperature changes in the mesosphere and stratosphere connected with circulation changes in winter, *J. Atmos. Sci.*, *29*, 756–766.

- Manney, G. L., K. Krüger, J. L. Sabutis, S. A. Sena, and S. Pawson (2005), The remarkable 2003–2004 winter and other recent warm winters in the Arctic stratosphere since the late 1990s, *J. Geophys. Res.*, *110*, D04107, doi:10.1029/2004JD005367.
- Manney, G. L., et al. (2008), The evolution of the stratopause during the 2006 major warming: Satellite data and assimilated meteorological analyses, *J. Geophys. Res.*, *113*, D11115, doi:10.1029/2007JD009097.
- Manson, A. H., et al. (2006), Winter warmings, tides and planetary waves: Comparisons between CMAM (with interactive chemistry) and MFR-MetO observations and data, *Ann. Geophys.*, *24*, 2493–2518.
- McLandress, C., and J. F. Scinocca (2005), The GCM response to current parameterizations of nonorographic gravity wave drag, *J. Atmos. Sci.*, *62*, 2394–2413.
- Miyoshi, Y. (2003), Effects of the sudden stratospheric warming on the temperature in the MLT region, *Adv. Polar Upper Atmos. Res.*, *17*, 1–12.
- Randall, C. E., et al. (2005), Stratospheric effects of energetic particle precipitation in 2003–2004, *Geophys. Res. Lett.*, *32*, L05802, doi:10.1029/2004GL022003.
- Randall, C. E., V. L. Harvey, C. S. Singleton, P. F. Bernath, C. D. Boone, and J. U. Kozyra (2006), Enhanced NO<sub>x</sub> in 2006 linked to strong upper stratospheric Arctic vortex, *Geophys. Res. Lett.*, *33*, L18811, doi:10.1029/2006GL027160.
- Rozanov, E., L. Callis, M. Schlesinger, F. Yang, N. Andronova, and V. Zubov (2005), Atmospheric response to NO<sub>y</sub> source due to energetic electron precipitation, *Geophys. Res. Lett.*, *32*, L14811, doi:10.1029/2005GL023041.
- Rusch, D. W., J.-C. Gérard, S. Solomon, P. J. Crutzen, and G. C. Reid (1981), The effect of particle precipitation events on the neutral and ion chemistry of the middle atmosphere – I. Odd nitrogen, *Planet. Space Sci.*, *29*, 767–774.
- Semeniuk, K., J. C. McConnell, and C. H. Jackman (2005), Simulation of the October–November 2003 solar proton events in the CMAM GCM: Comparison with observations, *Geophys. Res. Lett.*, *32*, L15S02, doi:10.1029/2005GL022392.
- Solomon, S., R. G. Roble, and P. Crutzen (1982), Photochemical coupling between the thermosphere and lower atmosphere: 1. Odd nitrogen from 50 to 120 km, *J. Geophys. Res.*, *87*, 7206–7220.
- Starkov, G. V. (1981), Statistical dependences between the magnetic activity indices, *Geomagn. Aeron.*, *34*, 101–103.
- Wennberg, P. O., J. G. Anderson, and D. K. Weisenstein (1994), Kinetics of reactions of ground state nitrogen atoms (<sup>4</sup>S<sub>3/2</sub>) with NO and NO<sub>2</sub>, *J. Geophys. Res.*, *99*, 18,839–18,846.
- Zhou, S., A. J. Miller, J. Wang, and J. K. Angell (2001), Downward-propagating temperature anomalies in the preconditioned polar stratosphere, *J. Clim.*, *15*, 781–792.

P. F. Bernath, Department of Chemistry, University of York, Heslington, York YO10 5DD, UK.

C. D. Boone, Department of Chemistry, University of Waterloo, Waterloo, ON N2L 3G1, Canada.

J. R. Jarosz, J. J. Jin, J. C. McConnell, and K. Semeniuk, Department of Earth and Space Science and Engineering, York University, Toronto, ON M3J 1P3, Canada. (kirill@nimbus.yorku.ca)